Earth, Planets and Space
a SpringerOpen Journal

FRONTIER LETTER Open Access

Geophysical assessment of migration and storage conditions of fluids in subduction zones

Anne Pommier

Abstract

By enhancing mass transfer and energy release, the cycle of volatiles and melt is a major component of subduction. Investigating this fluid cycle is therefore critical to understand the past and current activity of subduction zones. Fluids can significantly affect rock electrical conductivity and elastic parameters that are measured using electromagnetic and seismic methods, respectively. This letter emphasizes how these geophysical methods complement each other to provide information about the storage of fluids in subduction systems. By compiling electromagnetic and seismic results from various subduction zones, a possible correlation between electrical conductivity and seismic wave attenuation anomalies in the mantle wedge is observed, consistent with fluid accumulation. A possible relationship between geophysical properties and the slab age is also suggested, whereas no significant trend is observed between electrical conductivity or seismic wave attenuation and estimates of water flux in the mantle wedge. These field-based relationships require further constrains, emphasizing the need for new measurements in the laboratory.

Findings

Introduction

The dynamics and time-evolution of subduction are driven by mechanical and chemical processes that influence buoyancy forces, slab motion, contrasting thermal fields, phase equilibria, and volatile transport. By enhancing mass transfer and energy release, the cycle of fluids in subduction zones is a critical component of slab recycling and continental building processes. A better understanding of the role of melt and volatiles in subduction zones is therefore key to improving our knowledge of the geodynamic processes at work. It can also help us better assess volcanic and earthquake hazards in these contexts.

The cycle of fluids is expected to differ significantly between subduction zones. For instance, varying temperatures cause dehydration reactions to occur at shallower depths in the slabs of warm subduction zones (e.g., Southwest Japan, Cascades) compared to slabs of cold subduction zones (e.g., Tonga, Java) (Peacock and Wang 1999). Fluid migration was found to be faster than subduction velocity in warm subduction systems (e.g., approximately 7 cm/year versus approximately 4 cm/year, respectively, in Southwest Japan, Kawano et al. 2011), suggesting a continuous hydration of the mantle wedge due to upward fluid migration along the subduction interface. In colder environments, comparable fluid and subduction velocities (e.g., approximately 10 cm/year in Northeast Japan, Kawano et al. 2011) imply that a non-negligible amount of water reaches the lower mantle and triggers melting, as evidenced by geochemical signatures of island arc magmas (e.g., Stolper and Newman 1994; Wallace 2005). Significant water contents in the mantle are suggested by modeling studies. For instance, van Keken et al. (2011) estimated that the global H_2O flux to the deep mantle corresponds roughly to one ocean mass over the Earth's history.

Fluids influence electrical conductivity and seismic velocity in different ways (see Unsworth and Rondenay 2013). These physical properties are measured using electromagnetic and seismic methods, respectively, offering a unique way to map *in situ* fluid distributions in real time. When interpreted together with petrological results, geophysical data can be used to constrain fluid chemistry, temperature, fraction, and connectivity. Though some important findings have been obtained to relate electrical and seismic data to fluid distribution, thermal structure, and mineralogy (e.g., Kazatchenko et al. 2004; Hacker and Abers 2004; ten Grotenhuis et al. 2005), further work is required to understand the possible relationships between

Correspondence: apommier@asu.edu
School of Earth and Space Exploration, Arizona State University, Tempe, AZ 85287, USA

geophysical parameters sensitive to fluids and subduction dynamics.

This letter addresses how electromagnetic and seismic methods complement each other to help define the storage conditions of fluid processes in subduction. It aims to stimulate laboratory investigations that use a joint elec trical-seismic approach and combine geophysical data with subduction settings.

Geophysical structure of subduction zones and fluid detection

Electrical conductivity structure of subduction zones

Because it is sensitive to temperature, composition, and interconnectivity changes, the electrical conductivity of geomaterials provides information about their chemistry and structure (see Pommier 2013). Most electrical images of the subduction zones present two anomalies unnecessarily connected along or above the slab: a backarc conductor and a near-trench conductor (Table 1). These conductive areas are usually interpreted as zones of fluid accumulation, in agreement with petrological modeling (e.g., Schmidt and Poli 1998). The upward migration of fluids from the slab may explain backarc and forearc anomalies. In some subduction zones, the forearc conductor extends from the slab upward and can relate to the arc volcanoes' plumbing system (e.g., Brasse and Eydam 2008), whereas in other subduction contexts, conductivity images suggest a connection between the volcanic plumbing system and the backarc reservoir (e.g., Evans et al. 2013). The fluid fraction is usually estimated from the bulk electrical conductivity value of the anomaly by using two-phase formalisms (e.g., ten Grotenhuis et al. 2005) and by assuming a conductivity value for the liquid phase (preferentially based on laboratory results and in agreement with petrological constraints (Pommier and Garnero 2014)). It is interesting to note that these possible fluid sinks are not vertically aligned with the arc volcanoes at the surface (e.g., Worzewski et al. 2011), though they may be rela ted to the volcanic plumbing system. In case these conductive reservoirs contribute to the volcanic activity, the shift in their location may be due to mantle flow and buoyancy processes in the mantle wedge, as suggested by some numerical experiments (e.g., Gerya and Yuen 2003). The detection of these reservoirs using electromagnetic measurements highlights the fact that electrical studies can be a powerful tool to investigate volcanic plumbing systems in subduction.

Table 1 Location and average electrical conductivity (EC) of main conductors detected in electromagnetic studies of subduction zones

Subduction zone	Backarc conductor			Forearc or trench-close conductor			References
	Depth (km)	EC (S/m)	Distance from trench (km)	Depth (km)	EC (S/m)	Distance from trench (km)	
1. Chile-Bolivia (19.5°S-21°S)	20	0.04.-0.10	220		n.c.		Brasse et al. (2002)
2. Chile-Bolivia (17°S-19°S)	100	0.10-1	300		n.c.		Brasse and Eydam (2008)
3. Costa Rica	30	0.03-0.13	150	10	0.10-0.20	65	Worzewski et al. (2011)
4. Mexico	40	0.03-0.20	330	20	0.10-0.20	40	Joedicke et al. (2006)
5. Philippine Sea	85	0.50	320	40	0.50	140	Shimakawa and Honkura (1991)
6. South Chile	25	0.10-0.30	140	15	0.03-1	45	Brasse et al.(2009)
7. Central Argentina	200	0.03-1	800	30	0.02	300 or less	Booker et al. (2004)
8. Cascadia, British Columbia	50	0.02-0.05	120	25	0.02	50	Soyer and Unsworth (2006)
9. Cascadia, Oregon	80	0.03-1	120	25	0.03-1	80	Evans et al. (2013)
10. Greece	40	0.002-0.006	170	-	-	-	Galanopoulos et al. (2005)
11. Mariana	40	0.01	300	<30?	0.006?	50-150?	Matsuno et al. (2012)
12. Taiwan	35	0.0590.10	100	10	0.05-0.12	30	Bertrand et al. (2012)
13. Kyushu, Japan	50	1	300		n.c.		Ichiki et al. (2000)
14. Hokkaido, Japan	40	0.01-0.10	400	40	0.01-0.10	100	Ichiki et al. (2009)
15. North Honshu, Japan	170	0.15-0.30	260	15	0.10	210	Toh et al. (2006)
16. Central New Zealand	35	0.01-0.04	200	20	0.10	150	Wannamaker et al. (2009)

n.c, zone close to trench not covered by the electromagnetic survey.

Although conductive anomalies in subduction zones are almost systematically interpreted as interconnected fluids, other materials may present high electrical conductivity. In Figure 1, the electrical conductivity of fluids and other materials at conditions relevant to subduction is compared in a synthetic conductivity profile based on laboratory results. Petrological properties are from Schmidt and Poli (1998) for the slab and mantle wedge, and the thermal profile is derived from Furukawa (1993) and Poli and Schmidt (2002). Melt fraction estimates are from Grove et al. (2012). The electrical conductivity of these materials is calculated using the results by Kristinsdóttir et al. (2010) (chlorite), Wang et al. (2012) (amphibole), Zhu et al. (1999), Xie et al. (2002) and Guo et al. (2011) (serpentinite), Constable (2006) (olivine), and Ni et al. (2011) and Yoshino et al. (2010) (silicate melt). Because some of these electrical measurements were performed at lower pressure than subduction conditions, the effect of increasing pressure on conductivity was accounted for by applying a correction of −0.15 log unit in electrical conductivity per gigapascal, in agreement with observations from experimental studies (e.g., Tyburczy and Waff 1983). Tempe rature corrections were applied to measurements of electrical conductivities of chlorite. Those were made at temperatures <250°C, while petrology studies suggest that chlorite may be stable in the mantle wedge at significantly higher temperatures (up to 1,000°C) (Schmidt and Poli 1998). The electrical conductivity of chlorite at higher temperatures is predicted by extrapolation assuming a constant Arrhenian dependence to temperature over the temperature range of interest.

This synthetic model suggests that the contrast in electrical conductivity between stable hydrous minerals in the slab and the mantle can be less than 1 log unit. This observation is consistent with the results from magnetotelluric studies that can hardly distinguish the slab from the surrounding mantle and, therefore, often resort to seismic studies to locate the slab (Brasse and Eydam 2008; Naif et al. 2013). Figure 1B also predicts that the electrical response of hydrous minerals (chlorite, amphibole) may be similar to that of partial melt at conditions relevant to subduction, therefore hampering the identification of a free fluid phase. Improving our understanding of fluid distribution in subduction zones requires the integration of results from electromagnetic surveys with those from petrology and seismology.

Input from seismic studies

Different seismic techniques are used to probe subduction zones (see Unsworth and Rondenay 2013). Among the different seismic observables, a reduction in seismic velocities and quality factor Q can be used to infer fluid-bearing regions at depth and define fluid pathways (e.g., Syracuse et al. 2008; Rychert et al. 2008). In particular, seismic wave attenuation (Q^{-1}) and Poisson's ratio (V_p/V_s) are sensitive to the presence of fluid and high temperature (Takei 2002), and some models showed that seismic velocities can be related to the fluid content within the mantle wedge (e.g., Carlson and Miller 2003). Estimates of volume fraction of fluids have been proposed based on these seismic parameters, and further work is needed to place stronger quantitative constraints (Aizawa et al. 2008). Low seismic velocity zones are commonly detected at shallow depths in relatively warm subduction contexts (Hirose et al. 2008) and at higher depths in the mantle wedge of cold subduction environments (Tsuji et al. 2008). Seismic attenuation can be caused by mechanisms that are not all related to the presence of fluid, such as grain defect microdynamics, viscosity, and scattering (e.g., Johnston et al. 1979; Karato and Spetzler 1990). Therefore, the interpretation of seismic attenuation in terms of fluid requires its coupling with other fluid-dependent geophysical parameters.

Examples of seismic results in subduction are presented in Figure 2 and Table 2. In the Tonga/Lau system (Wiens et al. 2008; Pozgay et al. 2009), a low-attenuation slab and large-extent high attenuation regions have been observed in the forearc and backarc areas (Figure 2A). Attenuation studies possibly indicate the presence of free fluids or

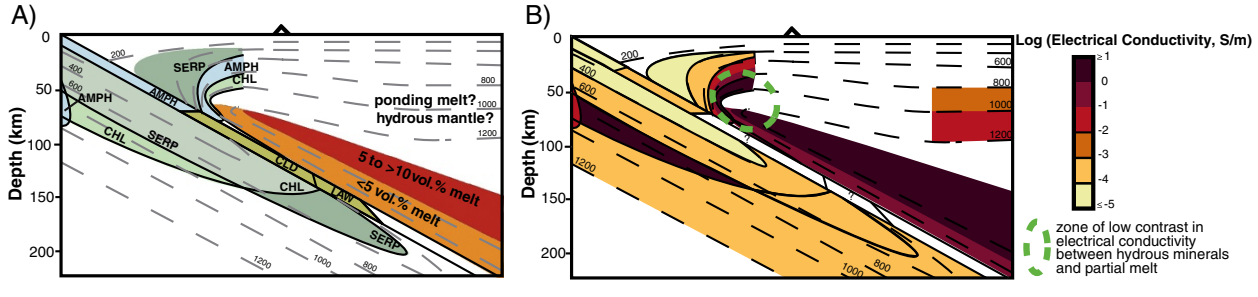

Figure 1 Laboratory-based electrical conductivity model of a subduction zone. (A) Considered mineralogy and thermal profile, after Schmidt and Poli (1998) and Grove et al. (2012). **(B)** Corresponding electrical response based on laboratory studies (see text for details). The green area underlines that the distinction between hydrous minerals and partially molten rocks is not possible based on electrical conductivity only, because these phases have similar electrical conductivity values at conditions relevant to subduction.

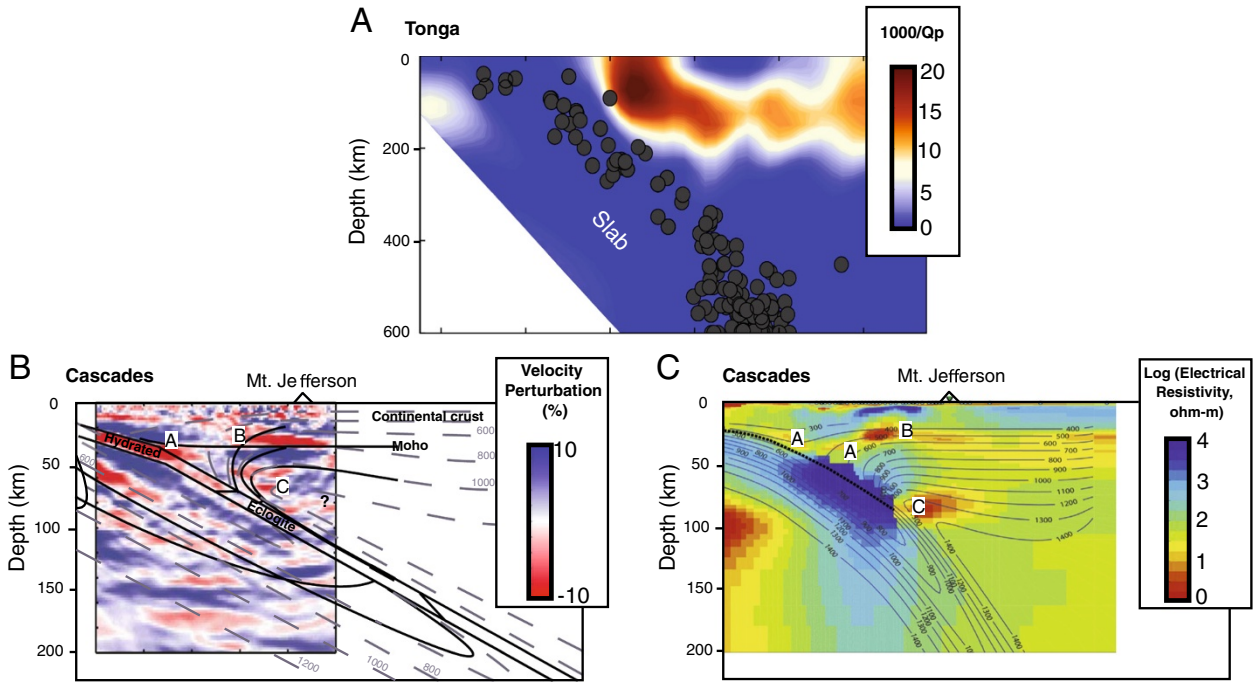

Figure 2 Examples of geophysical subduction profiles. (A) *P* wave attenuation tomography in the Tonga/Lau system (after Pozgay et al. 2009). Circles are earthquakes. **(B)** Seismic velocity contrast profile created using teleseisms. **(C)** Electromagnetic profiles of the Cascades (Rondenay et al. 2008; Evans et al. 2013). Labels A, B, and C correspond to possible fluid accumulation areas (forearc and backarc conductors). See text for details.

serpentinization, but it is important to keep in mind that the effect of fluid processes on attenuation is still poorly constrained.

The inversion of converted and scattered teleseismic waves method does not clearly identify the zones of fluid accumulation (e.g., Rondenay et al. 2010), but rather fronts of serpentinization (Bostock et al. 2002), whose location is consistent with thermal and petrological subduction models at shallow depth (<~70 km). Serpentinization of the slab and mantle wedge is ascribed to a series of dehydration reactions that lead to permanent changes in the mineralogy and represents a major component of the fluid cycle at shallow depth (e.g., Reynard 2013).

Beneath the Cascades (Figure 2B), several small low seismic velocity zones are present, but no pronounced low-velocity zone can be distinctly observed in the mantle wedge where partial melt is expected (Rondenay et al. 2008), whereas electrical data clearly identified conductive zones interpreted as fluid accumulation areas, noted as A, B, C (Figure 2C; Evans et al. 2013). Region A is consistent with the presence of fluids from slab dehydration at shallow depth, B with a zone of fluid accumulation possibly related to the volcanic plumbing system, and C is in agreement with the presence of deeper partial melting. These conductive anomalies correspond to zones of seismic velocity reduction in Figure 2B, but they could not be clearly identified on the seismic profile without additional constraints from the electromagnetic study.

Relating electrical and seismic parameters to map fluid distribution

Electrical conductivity-seismic velocity relationships in fluid-bearing materials

Attempts to relate electrical and seismic properties of fluid-bearing materials are scarce (Kazatchenko et al. 2004; Pommier and Garnero 2014). These petrophysical models are based on theoretical approaches and laboratory measurements and aim to improve the interpretation of geophysical data. Another approach would consist of exploring electrical conductivity-seismic velocity relationships by considering their values from field measurements.

Figure 3 compares attenuation values for seismic *P* and *S* waves for both forearc/trench-close and backarc anomalies and highest electrical conductivities in similar areas. These values are directly from the studies listed in Tables 1 and 2, and possible issues of resolution of the geophysical data are not considered here. A simple correlation between electrical conductivity (EC) and Q^{-1} values is observed:

$$\text{For } P \text{ waves}: \text{EC}(\text{S/m}) = 1.50.10^{-3} Q_p^{-1} - 0.104 \quad (1)$$

$$\text{For } S \text{ waves}: \text{EC}(\text{S/m}) = 1.20.10^{-3} Q_s^{-1} - 0.059 \quad (2)$$

Table 2 Location, highest seismic wave attenuation values, and wave velocity ratios of mantle wedge seismic anomalies

Subduction zone	Backarc anomaly					Forearc or trench-close anomaly					References
	Depth (km)	Attenuation			V_p/V_s	Depth (km)	Attenuation			V_p/V_s	
		f range (Hz)	*P* wave	*S* wave			*f* range (Hz)	*P* wave	*S* wave		
1. Mariana	50-75	0.10-9.5	93-132	63-76	-	25-50	0.10-9.5	63-93	42-56	-	Pozgay et al. (2009); Wiens et al. (2006)
2. Tonga-Lau	50-70	0.10-3.5	47-60	15-30	1.70	<20	-	-	-	?	Wiens et al. (2008)
3. NE Japan	30-100	1.0-8.0	-	70-120	1.85	<25	-	-	-	1.85	Zhao et al. (2007); Takanami et al. (2000)
4. Honshu, Japan	80-100	1.0-20?	150	-	-	30-60	1.0-20?	150-180	-	-	Tsumura et al. (2000)
5. Taiwan	60-80	0.15-8.0	100	-	-	-	-	-	-	-	Ko et al. (2012)
6. Central Java, Indonesia	70-120	1.0-20	100	-	-	30-50	1.0-20	<100	-	-	Bohm et al. (2013)
7. North New Zealand	40-100	2.0-40	50-120	-	-	<25	2.0-40	120-200	-	-	Eberhart-Phillips et al. (2008)
8. Mexico	40 and 80-120	1.0-30	130	-	-	20	1.0-30	160	-	-	Chen and Clayton (2009)
9. Nicaragua-Costa Rica	40-75	0.50-7.0	90-140	120-160	1.90	<50	0.50-7.0	125-200	125-200	1.90	Rychert et al. (2008); Dinc et al. (2011)
10. Central Andes −21, −22.1°S	50-150	1.0-7.0; 1.0-30	117	-	1.83	<60	1.0-7.0; 1.0-30	117	-	-	Myers et al. (1998); Schurr et al. (2003)
11. Central Andes −24.2°S	150-200	1.0-7.0; 1.0-30	105	-	-	30-100	1.0-7.0; 1.0-30	95	-	-	Schurr et al. (2003)
12. Alaska	80-100	1-19; 0.3-9	537	283	-	50-60	1-19; 0.3-9	<537	<283	-	Stachnik et al. (2004)

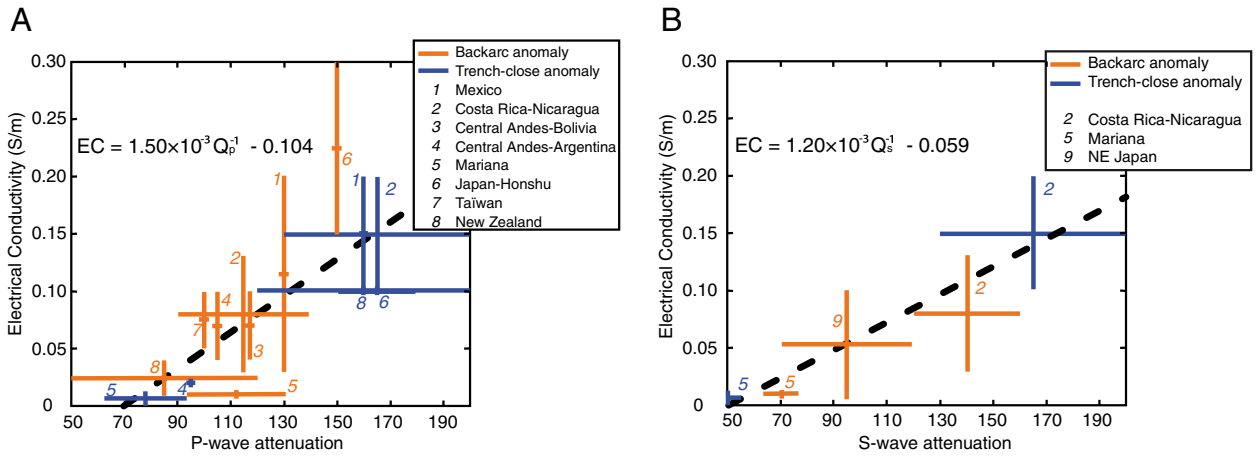

Figure 3 Electrical conductivity of anomalies of subduction zones versus *P* and *S* waves attenuation. Electrical conductivity of backarc (orange) and forearc (blue) anomalies of subduction zones versus *P* wave **(A)** and *S* wave **(B)** attenuation in similar areas. Values are from Tables 1 and 2. Both graphs suggest a relationship between electrical and seismic parameters.

with a correlation coefficient R of 0.78 for P waves and 0.96 for S waves. These relationships suggest that the higher the electrical conductivity of the anomaly, the higher its seismic attenuation, suggesting a plausible link in their cause.

Several and possibly combined causes can explain increases in electrical conductivity, Q_p^{-1}, and Q_s^{-1}. Because temperature affects both electrical and elastic parameters of fluid-bearing materials (e.g., Faul et al. 2004; ten Grotenhuis et al. 2005), thermal contrasts could explain the trend observed in Figure 3. For instance, the increase in EC between the Mariana electrical anomaly and the more conductive one in Honshu (difference of approximately 0.30 S/m, Table 1) can be explained by an increase from 1,200°C to 1,300°C, considering a hydrous basalt (6.3 wt.% H_2O) as the fluid phase (Ni et al. 2011), a melt fraction of 5%, and using the Hashin-Shtrikman upper bound (Hashin and Shtrikman 1962). The difference in seismic wave attenuation (Q_p^{-1} = 93 to 132 in Mariana, 150 in Honshu, Table 2) can be caused by a temperature change of 50°C (1,200°C to 1,250°C) or less on the corresponding frequency range according to the model by Faul et al. (2004) for a dunite containing 5% melt.

The geometry of the interconnected fluid phase in solid matrix can also explain the relationship between electrical conductivity and P wave and S wave attenuations. At defined fluid fraction, a change in fluid interconnectivity and geometry is likely to influence seismic velocities (S wave velocities more than P wave velocities, Watt et al. 1976), which will affect Poisson's ratio and increase seismic attenuation (e.g., Jackson et al. 2004). Fluid interconnectivity can also affect electrical conductivity significantly enough to explain the variations observed in Figure 3 (several tenths of S/m) (e.g., ten Grotenhuis et al. 2005). The spatial distribution of fluid can also be responsible for seismic and electrical anisotropy observed in the field (e.g., Kawakatsu et al. 2009; Caricchi et al. 2011), which is not considered in the present study.

Fluid composition affects electrical conductivity and may affect seismic velocities, though the effect of fluids (in particular, water) on seismic observables is poorly constrained and calibrated (Aizawa et al. 2008). The difference in electrical conductivity between the backarc anomaly in Honshu (>0.15 S/m) and in Mariana (approximately 0.01 S/m) (Table 1) is comparable to the conductivity increase caused by the addition of 7 wt.% H_2O to a basalt at 1,200°C, using the conductivity model by Ni et al. (2011). This would be consistent with the fact that the Mariana slab may have released most of its aqueous fluids, whereas the younger Honshu slab can still be expelling them, enriching partial melt accumulation zones with aqueous phase and leading to higher conductivity values.

An increase in the fluid content increases electrical conductivity (e.g., Nesbitt 1993), increases seismic wave attenuation (e.g., Jackson et al. 2004), and decreases seismic velocities (e.g., Mainprice 1997). Laboratory studies showed that electrical conductivity is very sensitive to fluid fraction (e.g., Caricchi et al. 2011; Yoshino et al. 2012), suggesting that a small change in fluid fraction can explain the differences in electrical conductivity between the different anomalies plotted in Figure 3 (assuming a similar temperature).

The relationship between electrical conductivity and seismic wave attenuation presented in Figure 3 suggests that the fluid conditions affect electrical conductivity and seismic wave attenuation in a similar manner, assuming that fluids are responsible for the electric and seismic signals. Further electrical and seismic investigations are needed to demonstrate if the slope (or intercept) of this empirical relationship depends on the amount of fluids

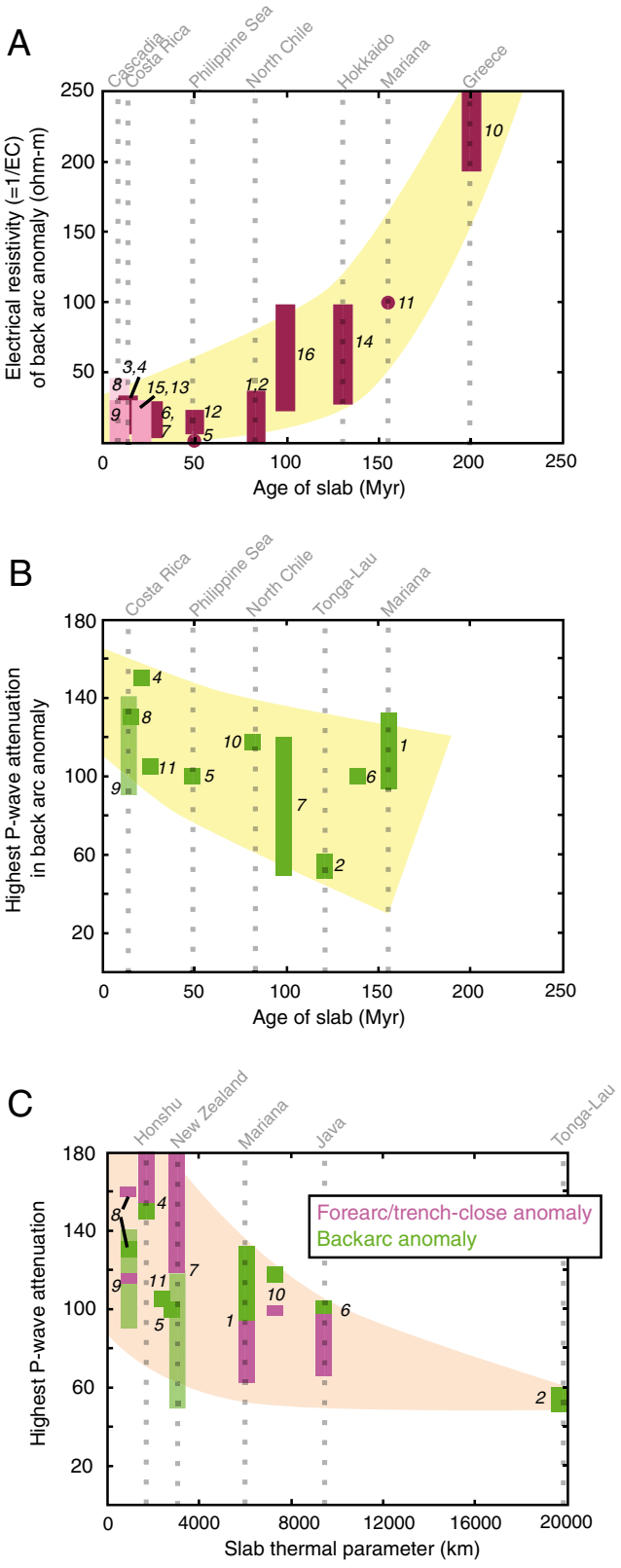

Figure 4 Geophysical parameters versus subduction settings. (A) Electrical response of backarc anomaly and slab age. **(B)** *P* wave attenuation in backarc anomaly and slab age. **(C)** *P* wave attenuation in backarc and forearc anomalies versus slab thermal parameter (see text for details). Shaded areas are a guide for the eye.

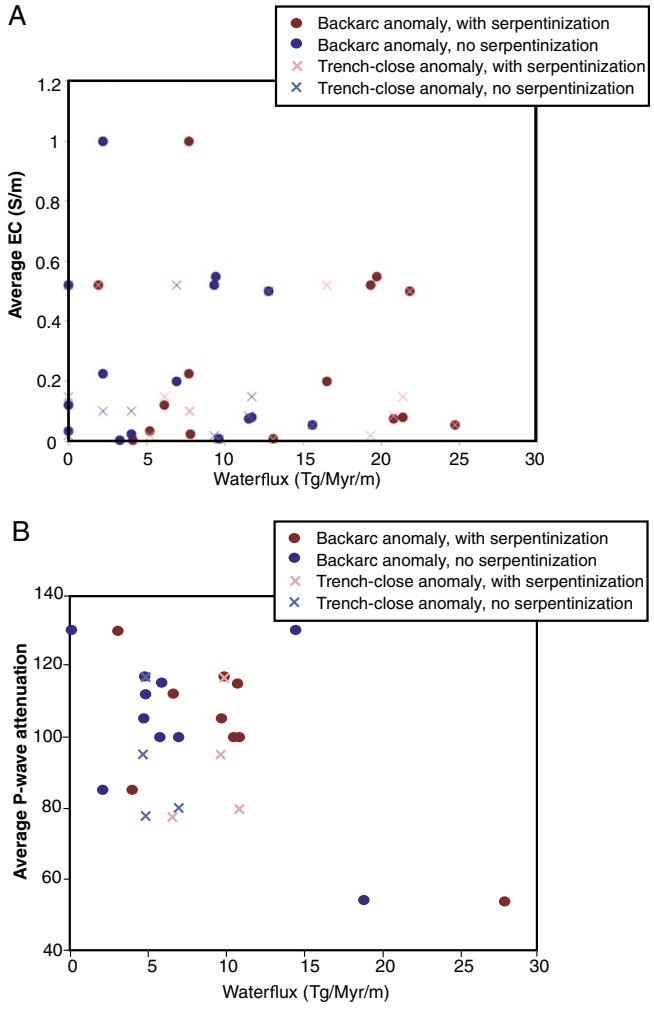

Figure 5 Water flux in backarc and trench-close anomalies versus electrical conductivity (A) and *P* wave attenuation (B). Water flux estimates from van Keken et al. (2011). No clear functional relationship is observed between water flux and conductivity or attenuation.

and their storage conditions and therefore place quantitative constraints on the nature of zones of fluid accumulation.

Relating electrical conductivity and seismic velocities to subduction settings

Using Tables 1 and 2, possible relationships between the values of geophysical parameters (electrical conductivity, Q^{-1}, V_p/V_s) of anomalies can be considered through their dependence on structural subduction characteristics (from Jarrard 1986 and van Keken et al. 2011). No significant correlation between electrical or seismic parameters and the distance from trench or the dip angle was observed. However, a correlation is possible between electrical conductivity (or its inverse, resistivity) and *P* wave attenuation of the backarc anomaly and the age of the slab (Figure 4), suggesting that the backarc anomaly is more conductive and the seismic waves are more attenuated when it is related to a young slab (<100 Myr) than to an older slab. This correlation seems more pronounced for electrical resistivity than for seismic wave attenuation. A low conductivity (or high resistivity) can correspond to a 'cooling' fluid and/or a small fluid fraction, possibly meaning a small extent of melting and accumulation.

Subduction settings can also be expressed through the slab thermal parameter (slab age × convergence speed) (Kirby et al. 1991). Its value is small for slow subduction of young lithosphere (e.g., Mexico, Cascades) and high for fast subduction of old lithosphere (e.g., Tonga, Java). No distinct relationship is observed between electrical conductivity of mantle wedge anomalies (forearc and backarc) and the slab thermal parameter. However, as underlined in Figure 4C, seismic wave attenuation tends to be higher for low slab thermal parameter values. This would be consistent with an abundant release of fluids related to the

dehydration process of a young crust, whereas the fast subduction of an old lithosphere does not promote fluid accumulation, leading to low seismic attenuation.

Geophysical parameters and global slab water flux

Geochemical studies proposed to estimate the fluxes of fluids (particularly water) in subduction, and models have been developed to estimate the amount of water expelled under compaction at shallow depth, as well as the amount of water reaching the deep mantle (e.g., Carlson and Miller 2003; van Keken et al. 2011).

Van Keken et al. (2011) estimated the H_2O flux at 100 km depth with and without serpentinization for the considered subduction zones. These fluxes are compared to the electrical and seismic properties of both trench-close and backarc anomalies (Figure 5). No significant trend is observed with high electrical conductivity in the mantle wedge (Figure 5A), and the same observation can be made about seismic wave attenuation (Figure 5B). The large uncertainties on fluid flux estimates do not allow the investigation of a possible relationship between the intensity of water fluxes in the mantle wedge and the geophysical properties of fluid reservoirs, highlighting the need for further laboratory and field investigations.

Concluding remarks: potential for improving the understanding of subduction settings using a joint electrical-seismic approach

Although thermo-mechanical models of subduction do not necessarily agree on the time-evolution, they all point out extreme temperature gradients across the slab-mantle interface (e.g., Syracuse et al. 2010). As underlined by Poli and Schmidt (2002), this suggests that a wide pressure-temperature-composition space has to be characterized to predict the evolution of subducting slabs. Because of the sensitivity of geophysical parameters to temperature and composition, electrical and seismic field studies, when combined with thermo-mechanical models, can be a useful tool to understand the pathways that led to the current state of a subduction system and may help define plausible scenarios for its evolution.

A few attempts combined the P-T paths of slabs from thermal models and phase equilibria on hydrous basalt or peridotite compositions (e.g., Poli and Schmidt 2002; Syracuse et al. 2010). Recently, Unsworth and Rondenay (2013) compared possible P-T paths of the slab with seismic velocity attenuation for a basaltic melt after Hacker (2008), attempting to relate dynamic models of subduction to the seismic properties of melt. Our knowledge of subduction would benefit from further joint investigations that promote the interpretation of seismic velocity and electrical conductivity in terms of composition and subduction dynamics. The recent expansion of geophysical experiments such as the EarthScope USArray seismic-magnetotelluric network offers the potential to improve significantly the relationships between electrical and elastic parameters.

Competing interests

The author declares that she has no competing interest.

Acknowledgements

This manuscript benefitted from discussions with and informal reviews by Stéphane Rondenay and Ed Garnero. Discussions with Kurt Leinenweber were also appreciated. The author thanks two anonymous reviewers for their comments.

Received: 3 February 2014 Accepted: 14 May 2014
Published: 23 May 2014

References

Aizawa Y, Barnhoorn A, Faul UH, Gerald JDF, Jackson I, Kovács I (2008) Seismic properties of Anita Bay dunite: an exploratory study of the influence of water. J Petrol 49(4):841–855, doi:10.1093/petrology/egn007

Bertrand EA, Bertrand EA, Unsworth MJ, Chiang CW, Chen CS, Chen CC, Wu FT, Türkoğlu E, Hsu HL, Hill GJ (2012) Magnetotelluric imaging beneath the Taiwan orogen: an arc-continent collision. J Geophys Res 117:B01402, doi:10.1029/2011JB008688

Bohm M, Haberland C, Asch G (2013) Imaging fluid-related subduction processes beneath Central Java (Indonesia) using seismic attenuation tomography. Tectonophys 590:175–188

Booker JR, Favetto A, Pomposiello MC (2004) Low electrical resistivity associated with plunging of the Nazca flat slab beneath Argentina. Nature 429:399–403

Bostock MG, Hyndman RD, Rondenay S, Peacock SM (2002) An inverted continental Moho and serpentinization of the forearc mantle. Nature 417:536–538

Brasse H, Eydam D (2008) Electrical conductivity beneath the Bolivian Orocline and its relation to subduction processes at the South American continental margin. J Geophys Res 113:B07109, doi:10.1029/ 2007JB005142

Brasse H, Lezaeta P, Rath V, Schwalenberg K, Soyer W, Haak V (2002) The Bolivian Altiplano conductivity anomaly. J Geophys Res 107(B5):2096, doi:10.1029/2001JB000391

Brasse H, Kapinos G, Li Y, Mütschard L, Soyer W, Eydam D (2009) Structural electrical anisotropy in the crust at the South–Central Chilean continental margin as inferred from geomagnetic transfer functions. Phys Earth Planet Int 173:7–16

Caricchi L, Gaillard F, Mecklenburgh J, Le Trong E (2011) Experimental determination of electrical conductivity during deformation of melt-bearing olivine aggregates: implications for electrical anisotropy in the oceanic low velocity zone. Earth Planet Sci Lett, doi:10.1016/j.epsl.2010.11.041

Carlson RL, Miller DJ (2003) Mantle wedge water contents estimated from seismic velocities in partially serpentinized peridotites. Geophys Res Lett 30(5):1250, doi:10.1029/2002GL016600

Chen T, Clayton RW (2009) Seismic attenuation structure in central Mexico: image of a focused high-attenuation zone in the mantle wedge. J Geophys Res 114:B07304, doi:10.1029/2008JB005964

Constable S (2006) SEO3: a new model of olivine electrical conductivity. Geophys J Int 166:435–437

Dinc AN, Rabbel W, Flueh ER, Taylor W (2011) Mantle wedge hydration in Nicaragua from local earthquake tomography. Geophys J Int 186:99–112

Eberhart-Phillips D, Reyners M, Chadwick M, Stuart G (2008) Three-dimensional attenuation structure of the Hikurangi subduction zone in the central North Island, New Zealand. Geophys J Int 174:418–434

Evans RL, Wannamaker PE, McGary RS, Elsenbeck J (2013) Electrical structure of the central Cascadia subduction zone: the EMSLAB Lincoln line revisited. Earth Planet Sci Lett, http://dx.doi.org/10.1016/j.epsl.2013.04.021

Faul UH, Fitz Gerald JD, Jackson I (2004) Shear wave attenuation and dispersion in melt-bearing olivine polycrystals: 2. Microstructural interpretation and seismological implications. J Geophys Res 109:B06202

Furukawa Y (1993) Magmatic processes under arcs and formation of the volcanic front. J Geophys Res 98:8309–8319

Galanopoulos D, Sakkas V, Kosmatos D, Lagios E (2005) Geoelectric investigation of the Hellenic subduction zone using long period magnetotelluric data. Tectonophys 409:73–84

Gerya TV, Yuen DA (2003) Rayleigh-Taylor instabilities from hydration and melting propel 'cold plumes' at subduction zones. Earth Planet Sci Lett 212:47–62
Grove TL, Till CB, Krawczynski MJ (2012) The role of H_2O in subduction zone magmatism. Annu Rev Earth Planet Sci 40:413–439
Guo X, Yoshino T, Katayama I (2011) Electrical conductivity anisotropy of deformed talc rocks and serpentinites at 3 GPa. Phys Earth Planet Int 188:69–81
Hacker BR (2008) H_2O subduction beneath arcs. Geochem Geophys Geosyst 9, doi:10.1029/2007GC001707
Hacker BR, Abers GA (2004) Subduction factory 3. An Excel worksheet and macro for calculating the densities, seismic wave speeds, and H_2O contents of minerals and rocks at pressure and temperature. Geochem Geophys Geosyst 5:Q01005, doi:10.1029/2003GC000614
Hashin Z, Shtrikman S (1962) A variational approach to the theory of the effective magnetic permeability of multiphase materials. J Appl Phys 33:3125–3131
Hirose F, Nakajima J, Hasegawa A (2008) Three-dimensional seismic velocity structure and configuration of the Philippine Sea slab in south western Japan estimated by double-difference tomography. J Geophys Res 113:B09315, doi:10.1029/2007JB005274
Ichiki M, Sumitomo N, Kagiyama T (2000) Resistivity structure of high-angle subduction zone in the southern Kyushu district, southwestern Japan. Earth Planets Space 52:539–548
Ichiki M, Baba K, Fuji-ta K (2009) An overview of electrical conductivity structures of the crust and upper mantle beneath the northwestern Pacific, the Japanese islands, and continental East Asia. Gondwana Res 16:545–562
Jackson I, Faul UH, Fitz Gerald FD, Tan BH (2004) Shear wave attenuation and dispersion in melt-bearing olivine polycrystals: 1. Specimen fabrication and mechanical testing. J Geophys Res 109:B06201
Jarrard RD (1986) Relations among subduction parameters. Rev Geophys 24(2):217–284
Joedicke H, Jording A, Ferrari L, Arzate J, Mezger K, Rüpke L (2006) Fluid release from the subducted Cocos plate and partial melting of the crust deduced from magnetotelluric studies in southern Mexico: implications for the generation of volcanism and subduction dynamics. J Geophys Res 111:B08102
Johnston DH, Toksoz MN, Timur A (1979) Attenuation of seismic-waves in dry and saturated rocks. 2. Mechanisms. Geophys J R Astron Soc 44(4):691–711
Karato S-I, Spetzler HA (1990) Defect microdynamics in minerals and solid state mechanisms of seismic wave attenuation and velocity dispersion in the mantle. Rev Geophys 28:399–421
Kawakatsu H, Kumar P, Takei Y, Shinohara M, Kanazawa T, Araki E, Suyehiro K (2009) Seismic evidence for sharp lithosphere–asthenosphere boundaries of oceanic plates. Science 324:499–502
Kawano S, Katayama I, Okazaki K (2011) Permeability anisotropy of serpentinite and fluid pathways in a subduction zone. Geology 39(10):939–942
Kazatchenko E, Markov M, Mousatov A (2004) Joint modeling of acoustic velocities and electrical conductivity from unified microstructure of rocks. J Geophys Res 109:B01202, doi:10.1029/2003JB002443
Kirby SH, Durham WB, Stern LA (1991) Mantle phase changes and deep earthquake faulting in subducted lithosphere. Science 252:216–225, doi:10.1126/science.252.5003.216
Ko Y-T, Kuo B-Y, Wang K-L, Lin S-C, Hung S-H (2012) The southwestern edge of the Ryukyu subduction zone: a high Q mantle wedge. Earth Planet Sci Lett 335–336:145–153
Kristinsdóttir LH, Flóvenz ÓG, Árnason K, Bruhn D, Milsch H, Spangenberg E, Kulenkampf J (2010) Electrical conductivity and P-wave velocity in rock samples from high-temperature Icelandic geothermal fields. Geotherm 39:94–105
Mainprice D (1997) Modelling the anisotropic seismic properties of partially molten rocks found at mid-ocean ridges. Tectonophys 279:161–179
Matsuno T, Evans RL, Seama N, Chave AD (2012) Electromagnetic constraints on a melt region beneath the central Mariana back-arc spreading ridge. Geochem Geophys Geosyst 13:Q10017, doi:10.1029/2012GC004326
Myers SC, Beck S, Zandt G, Wallace T (1998) Lithospheric-scale structure across the Bolivian Andes from tomographic images of velocity and attenuation for P and S waves. J Geophys Res 103:21233–21252
Naif S, Key K, Constable S, Evans RL (2013) Melt rich channel observed at the lithosphere–asthenosphere boundary. Nature 495:356–359, http://dx.doi.org/10.1038/nature11939
Nesbitt BE (1993) Electrical resistivities of crustal fluids. J Geophys Res 98:4301–4310
Ni H, Keppler H, Behrens H (2011) Electrical conductivity of hydrous basaltic melts: implications for partial melting in the upper mantle. Contrib Mineral Petrol 162:637–650
Peacock S, Wang K (1999) Seismic consequences of warm versus cool subduction metamorphism: examples from southwest and northeast Japan. Science 286(5441):937–939
Poli S, Schmidt M (2002) Petrology of subducted slabs. Annu Rev Earth Planet Sci 30:207–235
Pommier A (2013) Interpretation of magnetotelluric results using laboratory measurements. Surv Geophys, doi:10.1007/s10712-013-9226-2
Pommier A, Garnero EJ (2014) Petrology-based modeling of mantle melt electrical conductivity and joint-interpretation of electromagnetic and seismic results. J Geophys Res, doi:10.1002/2013JB010449
Pozgay SH, Wiens DA, Conder JA, Shiobara H, Sugioka H (2009) Seismic attenuation tomography of the Mariana subduction system: implications for thermal structure, volatile distribution, and slow spreading dynamics. Geochem Geophys Geosyst 10(4):Q04X05, doi:10.1029/2008GC002313
Reynard B (2013) Serpentine in active subduction zones. Lithos 178:171–185
Rondenay S, Abers GA, van Keken PE (2008) Seismic imaging of subduction zone metamorphism. Geology 36(4):275–278
Rondenay S, Montési LGJ, Abers GA (2010) New geophysical insight into the origin of the Denali volcanic gap. Geophys J Int 182:613–630
Rychert C, Fischer KM, Abers GA, Plank T, Syracuse E, Protti JM, Gonzalez V, Strauch W (2008) Strong Alon arc variation in attenuation in the mantle wedge beneath costa Rica and Nicaragua. Geochem Geophys Geosyst 9: Q10S10, doi:10.1029/2008GC002040
Schmidt MW, Poli S (1998) Experimentally based water budgets for dehydrating slabs and consequences for arc magma generation. Earth Planet Sci Lett 163:361–379
Schurr B, Asch G, Rietbrock A, Trumbull RB, Haberland C (2003) Complex patterns of fluid and melt transport in the central Andean subduction zone revealed by attenuation tomography. Earth Planet Sci Lett 215:105–119
Shimakawa Y, Honkura Y (1991) Electrical conductivity structure beneath the Ryukyu trench-arc system and its relation to the subduction of the Philippine sea plate. J Geomagnetism Geoelectricity 43:1–20
Soyer W, Unsworth M (2006) Deep electrical structure of the northern Cascadia (British Columbia, Canada) subduction zone: implications for the distribution of fluids. Geology 34(1):53–56, doi:10.1130/G21951.1
Stachnik JC, Abers GA, Chistensen DH (2004) Seismic attenuation and mantle wedge temperatures in the Alaska subduction zone. J Geophys Res 109:B10304
Stolper E, Newman S (1994) The role of water in the petrogenesis of Mariana trough magmas. Earth Planet Sci Lett 121:293–325
Syracuse EM, Abers GA, Fischer K, MacKenzie L, Rychert C, Protti M, Gonzalez V, Strauch W (2008) Seismic tomography and earthquake locations in the Nicaraguan and costa Rican upper mantle. Geochem Geophys Geosyst 9: Q07S08, doi:10.1029/2008GC001963
Syracuse EM, van Keken PE, Abers GA (2010) The global range of subduction zone thermal models. Phys Earth Planet Int 183:73–90
Takanami T, Sacks IS, Hasegawa A (2000) Attenuation structure beneath the volcanic front in northeastern Japan from broad-band seismograms. Phys Earth Planet Int 121:339–357
Takei Y (2002) Effect of pore geometry on Vp/Vs: from equilibrium geometry to crack. J Geophys Res 107(B2):2043, doi:10.1029/2001JB000522
ten Grotenhuis SM, Drury MR, Spiers CJ, Peach CJ (2005) Melt distribution in olivine rocks based on electrical conductivity measurements. J Geophys Res 110:B12201, doi:10.1029/2004JB003462
Toh H, Baba K, Ichiki M, Motobayashi T, Ogawa Y, Mishina M, Takahashi I (2006) Two-dimensional electrical section beneath the eastern margin of Japan Sea. Geophys Res Lett 33:L22309, doi:10.1029/2006GL027435
Tsuji Y, Nakajima J, Hasegawa A (2008) Tomographic evidence for hydrated oceanic crust of the pacific slab beneath northeastern Japan: implications for water transportation in subduction zones. Geophys Res Lett 35:L14308, doi:10.1029/2008GL034461
Tsumura N, Matsumoto S, Horiuchi S, Hasegawa A (2000) Three-dimensional attenuation structure beneath the northeastern Japan arc estimated from spectra of small earthquakes. Tectonophys 319:241–260
Tyburczy JA, Waff HS (1983) Electrical conductivity of molten basalt and andesite to 25 kilobars pressure: geophysical significance and implications for charge transport and melt structure. J Geophys Res 88(B3):2413–2430
Unsworth M, Rondenay S (2013) Actively observing fluid movement in the mid to deep crust and lithospheric mantle utilizing geophysical methods, solicited chapter. In: Harlov D, Austrheim H (eds) Metasomatism and metamorphism: the role of fluids in crustal and upper mantle processes. Lecture Notes in Earth System Sciences, Springer, pp 535–598, ISSN: 2193-8571

van Keken PE, Hacker B, Syracuse EM, Abers GA (2011) Subduction factory: 4. Depth-dependent flux of H_2O from subducting slabs worldwide. J Geophys Res 116:B01401, http://dx.doi.org/10.1029/2010JB007922

Wallace PJ (2005) Volatiles in subduction zone magmas: concentrations and fluxes based on melt inclusion and volcanic gas data. J Volc Geotherm Res 140:217–240

Wang D, Guo Y, Yu Y, Karato S-I (2012) Electrical conductivity of amphibole-bearing rocks: influence of dehydration. Contrib Mineral Petrol 164:17–25

Wannamaker PE, Caldwell TG, Jiracek GR, Maris V, Hill GJ, Ogawa Y, Bibby HM, Bennie SL, Heise W (2009) Fluid and deformation regime at an advancing subduction system at Marlborough, New Zealand. Nature 460:733–737

Watt JP, Davies GF, O'Connell RJ (1976) The elastic properties of composite materials, Rev. Geophys Space Phys 14(4):541–563

Wiens DA, Kelley K, Plank T (2006) Mantle temperature variations beneath back-arc spreading centers inferred from seismology, petrology, and bathymetry. Earth Planet Sci Lett 248:30–42

Wiens DA, Conder JA, Faul UH (2008) The seismic structure and dynamics of the mantle wedge. Annu Rev Earth Planet Sci 36:421–455

Worzewski T, Jegen M, Kopp H, Brasse H, Castillo WT (2011) Magnetotelluric image of the fluid cycle in the Costa Rican subduction zone. Nat Geosci 4:108–111

Xie H, Zhou W, Zhu M, Liu Y, Zhao Z, Guo J (2002) Elastic and electrical properties of serpentinite dehydration at high temperature and high pressure. J Phys Condens Matter 14:11359–11363

Yoshino T, Laumonier M, McIsaac E, Katsura T (2010) Electrical conductivity of basaltic and carbonatite melt-bearing peridotites at high pressures: implications for melt distribution and melt fraction in the upper mantle. Earth Planet Sci Lett 295:593–602

Yoshino T, McIsaac E, Laumonier M, Katsura T (2012) Electrical conductivity of partial molten carbonate peridotite. Phys Earth Planet Int 194–195:1–9

Zhao D, Wang Z, Umino N, Hasagawa A (2007) Tomographic imaging outside a seismic network: application to the northeast Japan arc. Bull Seismol Soc Am 97:1121–1132

Zhu M, Xie H, Guo J, Zhang Y, Xu Z (1999) Electrical conductivity measurement of serpentine at high temperature and pressure. Chin Sci Bull 44:1903–1907

doi:10.1186/1880-5981-66-38
Cite this article as: Pommier: **Geophysical assessment of migration and storage conditions of fluids in subduction zones.** *Earth, Planets and Space* 2014 **66**:38.